RSC Advances

PAPER

View Article Online
View Journal | View Issue

Cite this: *RSC Adv.*, 2014, **4**, 25040

A smart artificial glutathione peroxidase with temperature responsive activity constructed by host–guest interaction and self-assembly†

Yanzhen Yin,*[a] Shufei Jiao,[a] Chao Lang[b] and Junqiu Liu*[b]

Received 4th March 2014
Accepted 20th May 2014

DOI: 10.1039/c4ra04042b

www.rsc.org/advances

A smart supramolecular artificial glutathione peroxidase (**GPx**) with tunable catalytic activity was prepared based on host–guest interaction and a blending process. The functional guest molecules **ADA-Te** with catalytic center, **ADA-Arg** with binding site and the cyclodextrin-containing host polymers (**CD-PNIPAMs**) were first synthesized. The artificial glutathione peroxidase was constructed by host–guest interaction of **ADA-Te** and a series of **CD-PNIPAMs** with different molecular weights. Through altering the molar ratio of building blocks (**CD-PNIPAM$_{73}$**, **ADA-Te**, **ADA-Arg**), the optimum artificial **GPx** (**SGPx$_{max}$**) with vesicle structure was prepared *via* a blending process. Significantly, **SGPx$_{max}$** displayed a noticeable temperature responsive catalytic activity and exhibited typical saturation kinetics behavior of a real enzyme catalyst. It was proved that the change of the self-assembled structure of **SGPx$_{max}$** during the temperature responsive process played a significant role in altering the temperature responsive catalytic behavior. The construction of **SGPx$_{max}$** not only overcomes the insurmountable disadvantages existing in traditional supramolecular artificial **GPxs** but also bodes well for development of other biologically related functional supramolecular biomaterials.

Introduction

Reactive oxygen species (ROS) are the byproducts of cellular metabolism. The surplus ROS can lead to many human oxidative stress-related diseases.[1–3] Generally, such oxidative stress-related diseases are controlled by the antioxidative defense system, especially by the antioxidative enzyme system. As a member of the family of antioxidative enzymes, glutathione peroxidase (**GPx**, Ec.1.11.1.9) is an important selenium-containing enzyme, which catalyzes the reduction of hydroperoxides (ROOHs) using glutathione (GSH) as substrate.[4,5] Owing to its biologically crucial role, considerable efforts have been devoted to produce organoselenium/tellurium compounds that mimic the property of **GPx** in recent years.[6–12] In our group, based on the understanding of the structure of native **GPx**, some artificial **GPxs** have been designed based on macromolecular scaffolds.[13–20,45] Especially, considerable attentions have been drawn to artificial **GPxs** based on supramolecular scaffolds.[9,10,17,18,21,22]

Generally, molecular self-assembly behavior is a general phenomenon in nature, which plays a pivotal role in biological functions.[23,24] Being the alternative to the self-assembly structure in nature, versatile materials based on supramolecular chemistry have emerged as fascinating scaffolds for many interdisciplinary materials.[25–32] Typically, supramolecular materials are extensively applied in the fields of protein supramolecular complexes,[33,34] sensors,[35–37] controlled release systems,[38–41] artificial enzymes[18,21] as well as self-healing materials.[42,43] The unique properties of reversible dynamic assembly behavior and simplified construction process are all exhibited in these versatile materials. Specially, these unique properties are benefited to the construction of highly efficient supramolecular artificial **GPxs** (**SGPxs**). Liu and coworkers pioneered in the construction of the host **SGPx** with highly catalytic ability and strong substrate binding ability, which opened a new window for the preparation of artificial **GPx** based on supramolecular chemistry.[7,44] Subsequently, by marrying the successfully host cyclodextrin **GPx** with versatile supramolecular building blocks, **SGPxs** based on giant nanotube,[21] protein nanowire,[9] protein nanodisk,[10] supramolecular microgel,[45] hyperbranched supramolecular polymer[18] and star-shaped pseudo-block copolymer[19] were constructed. Similar to the traditional polymer scaffold for artificial enzyme, **SGPxs** were also proved to be endowed with the advantages of the simplified construction process as well as the enriched catalytic center.[46,47] Although supramolecular self-assembled materials were excellent scaffolds for artificial **GPx**, there were still two serious

[a]*School of Chemistry and Chemical Engineering, Qinzhou University, No.89, Xihuan Nanlu, Qinzhou 535000, People's Republic of China. E-mail: yinyanzhen2013@163.com; Fax: +86-0777-2860226*

[b]*State Key Laboratory of Supramolecular Structure and Materials, Jilin University, Changchun 130012, People's Republic of China. E-mail: junqiuliu@jlu.edu.cn; Fax: +86-43185193421*

† Electronic supplementary information (ESI) available: The synthesis of **ADA-Te**, **ADA-Arg**, **CD-Br** and **CD-PNIPAM**. See DOI: 10.1039/c4ra04042b

disadvantages in these **SGPxs**. On the one hand, most of them were just endowed with the catalytic center of **GPx**, which was only one of the three catalytic factors functioned to maintain the high catalytic activity.[9,10,19] It was a pity that the binding sites were usually absence, which could not accurately mimic the catalysis and recognition of native **GPx**. On the other hand, even if the binding sites and catalytic center were both anchored into a few of **SGPxs**, the intelligent alteration of substrate binding ability and catalytic ability could not be achieved.[18,21] It was known that only surplus ROS led to many human oxidative stress-related diseases and appropriate amount of ROS commonly acted as signal molecules in the metabolism.[1,3] The absence of adjustable and intelligent catalytic ability in **SGPx** has largely limited the further investigation and application of artificial **GPx**. Therefore, how to overcome these two disadvantages, design a novel **SGPx** with adjustable catalytic ability and bearing enriched catalytic factors (catalytic center and substrate binding sites) is still a great challenge.

Blending process is a versatile strategy exploited for the development of new polymeric materials with property profiles superior to those of the individual components.[20,48–50] The unique property of blending process can be employed to overcome the disadvantage of the absence of enriched catalytic factors. Moreover, in our previous reports, we also proved that the construction of smart artificial **GPx** with intelligent catalytic ability was achievable using traditional single chain block copolymer and supramolecular microgel as scaffolds based on PNIPAM.[45,50] Therefore, the application of the construction method from previous intelligent artificial **GPx** in the development of novel **SGPx** is desirable. It can overcome the disadvantage of absence of the intelligent catalytic ability in previous **SGPxs**. Additionally, the host–guest interaction between cyclodextrin and adamantine has been proved to be the efficient noncovalent interaction for the construction of supramolecular materials.[42–51]

Herein, we designed a novel smart **SGPx** combining PNIPAM scaffold, host–guest interaction self-assembly and blending process. Typically, as a novel smart artificial **GPx**, $\mathbf{SGPx_{max}}$ displayed a noticeable temperature responsive catalytic activity and the typical saturation kinetics behavior as a real enzyme catalyst. To the best of our knowledge, this is the first example of the successful construction of smart artificial **GPx** based on host–guest interaction and a blending process. We anticipate that this artificial **GPx** not only bodes well for the exploration of intelligent antioxidant drugs but also highlights the development of host–guest self-assembled supramolecular materials.

Experimental section

Materials

Tris(2-aminoethyl)amine (TREN, Acros) was used as received. Tris(2-dimethylaminoethyl)amine (Me_6TREN) was synthesized as described previously.[52] *N*-Isopropylacrylamide (NIPAM) (Aldrich) was recrystallized from hexane and toluene, and dried under a vacuum prior to use. Sodium borohydride, 1-adamantanecarbonyl chloride, and 3-bromo-1-propanol were purchased from Fluka and were used without further purification. Cumene hydorperoxide (CUOOH), H_2O_2, and 4-nitrobenzenethiol (NBT) were purchased from J&K Scientific Ltd. 3-Carboxyl-4-nitrobenzenethiol (TNB) was synthesized from 5,5′-dithiobis(2-nitrobenzoic acid) as described previously.[7] Acrylamide, L-arginine, 1-adamantanecarbonyl chloride, tellurium powder, β-cyclodextrin, phenyl methanol and 4-toluene sulfonyl chloride were purchased from Shanghai Reagent Co. Acryloyl chloride and propargyl alcohol were purchased from Anhui Wotu Reagent Co. 2-Bromopropanoly bromide was purchased from Lancaster. Triethylamine and tetrahydrofuran were rigorously dried with sodium. 1-[*p*-(Phenyl-azo) phenoxyethyl]pyridinium bromide (**AZO**) was endowed from Liu's group (**AZO**: 1H NMR (300 MHz, $(CD_3)_2SO$) δ (ppm) 9.17 (d, 2H), 8.66 (t, 1H), 8.21 (t, 2H), 7.90–7.81 (m, 4H), 7.60–7.52 (m, 3H), 7.13 (d, 2H), 5.10 (t, 2H), 4.65 (t, 2H).).

Instrumentations

The characterization of the structures of the compounds was performed with Bruker 300 MHz spectrometer using a TMS proton signal as the internal standard. UV-vis spectra were obtained using a Shimadzu 2450 UV-vis-NIR spectrophotometer. Scanning electron microscopy (SEM) observations were carried out on a JEOL JSM-6700F scanning electron microscope with primary electron energy of 3 kV. Transmission electron microscopy (TEM) observations were carried out on a JEOL JEM 3010 scanning electron microscope. The buffer pH values were determined with a METTLER TOLEDO 320 pH meter. Dynamic light scattering experiments were performed at Malven ZETAS12-ERNANOSERIES instrument. Molecular weights and molecular weight distributions were determined by GPC using THF as eluent at a flow rate of 1.0 mL min^{-1}.

The synthesis of **ADA-Te**, **ADA-Arg**, **CD-Br** were given in ESI.† **CD-PNIPAMs** were synthesized according to the polymerization procedure reported by Masci *et al.*[53] The detailed synthesis process was available in ESI.†

Determination of the LCST

The determination of LCST was carried out according to the previous reported method.[54] Typically, the optical transmissions of **CD-PNIPAM** solution (1 mg mL^{-1}) at different temperatures were measured at 600 nm using a Shimadzu 2450 UV-vis-NIR spectrophotometer. Sample cells were thermostated in a circulator bath at different temperatures from 25 to 45 °C prior to the measurements. The LCST was defined as the temperature of the 50% transmittance point during the first heating ramp.

Preparation of Te-CD-PNIPAM$_{73}$

The supramolecular building block **Te-CD-PNIPAM$_{73}$** with catalytic center of **GPx** was prepared based on **ADA-Te** and **CD-PNIPAM$_{73}$**. Typically, the preparation process was like this: **ADA-Te** (8.16 mg, 0.02 mmol) was dissolved in 0.20 mL DMF. **CD-PNIPAM$_{73}$** (196.3 mg, 0.02 mmol) was dissolved in 3.80 mL deionized water. Then, DMF solution of **ADA-Te** was slowly added into the solution of **CD-PNIPAM$_{73}$** under sonication at 25 °C. After the dropwise process was finished, the mixture

solution was treated under continual sonication at 25 °C for 20 min. Then, the solution was removed by a rotary evaporator and the product was dried under vacuum for 24 h at 45 °C. Finally, the dried product was dissolved in 10 mL PBS. And **Te-CD-PNIPAM$_{73}$** with the concentration of 2 mM was obtained.

Preparation of Arg-CD-PNIPAM$_{73}$

The preparation process of **Arg-CD-PNIPAM$_{73}$** was similar to that of **Te-CD-PNIPAM$_{73}$** except that **ADA-Te** was replaced by **ADA-Arg**. And **Arg-CD-PNIPAM$_{73}$** with the concentration of 2 mM was obtained.

Determination of GPx activity

The catalytic activity was assayed according to a modified method reported by Hilvert *et al.*[12] Typically, the reaction was carried out at 36 °C in a 1 mL quartz cuvette, 700 μL of phosphate buffer (pH = 7.0, 50 mM) and 100 μL of **SGPx$_{max}$** (10 μM) were added, and then 100 μL of the TNB solution (1.5 mM) was added. The mixture in the quartz cuvette was pre-incubated at appropriate temperature for 3 min. Finally, the reaction was initiated by the addition of 100 μL of cumene hydroperoxide (CUOOH) (2.5 mM), and the absorption decrease of TNB at 410 nm (ε_{410} = 13 600 M^{-1} cm^{-1}, pH = 7.0) was monitored using a Shimadzu 2450 UV-vis-NIR spectrophotometer. Appropriate control of the non-enzymatic reaction was performed and was subtracted from the catalyzed reaction.

Results and discussion

Construction of supramolecular building blocks for artificial GPx

The crystal structure of bovine erythrocyte glutathione peroxidase was reported by Epp *et al.* in 1983.[4] And the catalytic site of **GPx** has been well studied. It was suggested that three important catalytic factors contributed to maintaining the efficient **GPx** catalytic activity: catalytic center, binding site, and hydrophobic cavity. Based on our previous studies, tellurium, arginine derivative and cyclodextrin were selected as efficient alternative catalytic factors in artificial **GPx.**[14–20] As shown in Table 1, the description of abbreviation in this work was illustrated. As displayed in Fig. 1, **ADA-Te** with a similar function of selenocysteine was prepared as a catalytic center. **ADA-Arg** was responsible for the complexation of carboxyl groups of substrates as the binding site. Considering that ATRP was the efficient controlled polymerization for the synthesis of functional polymers,[55,56] various cyclodextrin-containing host polymers (**CD-PNIPAMs**) with different molecular weights were synthesized by ATRP (see Fig. 2). GPC measurement displayed that their degree of polymerization (DPs) were estimated to be 73, 130, 374, respectively (see ESI†). And the corresponding **CD-PNIPAMs** were denoted as **CD-PNIPAM$_{73}$**, **CD-PNIPAM$_{130}$**, **CD-PNIPAM$_{374}$**, respectively. Herein, **CD-Br** was the macroinitiator and contributed to anchoring the cyclodextrin into **CD-PNIPAMs**. Typically, the cyclodextrin end group in **CD-PNIPAMs** served as two purposes: on the one hand, it acted as host molecule for including guest molecules (**ADA-Te** or **ADA-Arg**) in the host–guest complex; on the other hand, the hydrophobic cavity of cyclodextrin in **SGPx** provided the hydrophobic microenvironment for the binding of hydrophobic substrates.

PNIPAM undergoes a reversible volume phase transition at near-physiological temperature, which is a thermally sensitive polymer with a lower critical solution temperature (LCST) of 32 °C.[57,58] Therefore, during the temperature responsive process, the soluble block copolymer bearing PNIPAM block can change to amphiphilic polymer when PNIPAM block shifts

Table 1 Description of abbreviation in this work

Abbreviation	Description
GPx	Glutathione peroxidase
ADA-Te	Guest molecules with catalytic center (see Fig. 1)
ADA-Arg	Guest molecules with binding site (see Fig. 1)
CD-PNIPAMs	Cyclodextrin-containing host polymers (see Fig. 2)
SGPxs	Supramolecular artificial **GPxs**
AZO	1-[*p*-(Phenyl-azo) phenoxyethyl]pyridinium bromide(see Scheme 2)
Te-CD-PNIPAM$_{73}$	Complex of **ADA-Te** and **CD-PNIPAM$_{73}$.**
Te-CD-PNIPAM$_{130}$	Complex of **ADA-Te** and **CD-PNIPAM$_{130}$**
Te-CD-PNIPAM$_{374}$	Complex of **ADA-Te** and **CD-PNIPAM$_{374}$**
Arg-CD-PNIPAM$_{73}$	Complex of **ADA-Arg** and **CD-PNIPAM$_{73}$.**
CD-Te-CD-PNIPAM$_{73}$	Blend of **CD-PNIPAM$_{73}$** and **Te-CD-PNIPAM$_{73}$**
Arg-Te-CD-PNIPAM$_{73}$	Blend of **Arg-PNIPAM$_{73}$** and **Te-CD-PNIPAM$_{73}$**
SGPx$_{max}$	Optimum artificial **GPx** by blend of **CD-PNIPAM$_{73}$** and **Te-CD-PNIPAM$_{73}$**

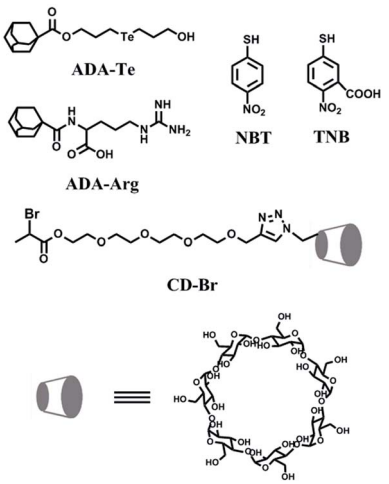

Fig. 1 The structures of the functional monomers ADA-Te, ADA-Arg, CD-Br and substrates (NBT, TNB).

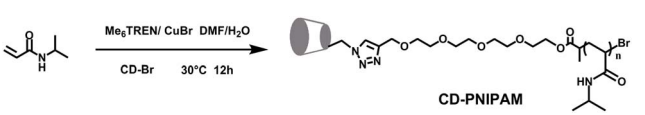

Fig. 2 Synthesis of CD-PNIPAM.

from being hydrophilic to hydrophobic. It provides the platform for the construction of versatile self-assembled materials.[16,59,60] For **SGPx** in this work, the temperature responsive property of its PNIPAM scaffold plays an important role in the adjusting of catalytic activity. Based on the functional building blocks (**CD-PNIPAM$_{73}$**, **ADA-Te**, **ADA-Arg**), **SGPx** was constructed and illustrated in Scheme 1. Firstly, base on the host–guest interaction between adamantane (guest molecule in **ADA-Te** or **ADA-Arg**) and cyclodextrin (host molecule in **CD-PNIPAM**), the supramolecular building blocks (**Te-CD-PNIPAM$_{73}$**, **Arg-CD-PNIPAM$_{73}$**) with **GPx** catalytic factors were prepared and given in Scheme 1 section 1. Secondly, **SGPx$_{max}$** was constructed by a blending process (see Scheme 1 section 2). Finally, the reversible temperature responsive property of **SGPx$_{max}$** was illustrated in Scheme 1 section 3.

To prove the formation of host–guest complex in **SGPx**, NMR assay was carried out using **AZO** as an indicator. It is known that the host–guest complex between adamantane and cyclodextrin is remarkable stable. And the host–guest interaction between **AZO** and cyclodextrin is relative weak. Therefore, the graphical representation of the assumed competitive complex mechanism was given in Scheme 2.

To confirm this hypothesis, three groups of ^{1}H NMR spectra were characterized and illustrated in Fig. 3. Among three groups of ^{1}H NMR spectra, **complex 1** was the proton signals of aromatic rings in the binary system of **AZO + CD-PNIPAM$_{73}$**, **complex 2** was the proton signals of aromatic rings in the ternary system of **AZO + Te-CD-PNIPAM$_{73}$**, and **complex 3** was the aromatic rings in the ternary system of **AZO + Arg-CD-PNIPAM$_{73}$** in D_2O. Comparing **complex 1** with **complex 2** or **complex 3**, we noticed that proton signals of c_1, a_1, b_1, h_1 in **complex 1** shifted to a low field, which suggested that these protons were exposed to water moderately. This phenomenon might be derived from the better solubility of **AZO** when it was included in the hydrophobic cavity of cyclodextrin. We also found that proton signals of d_1 and g_1 in **complex 1** shifted to a high field (proton signals of e_1 and f_1 were buried by the protons of polymer), which suggested that these protons were included in

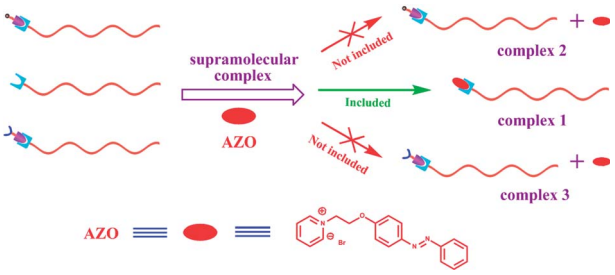

Scheme 2 A graphical representation of the competitive complex mechanism using AZO as an indicator.

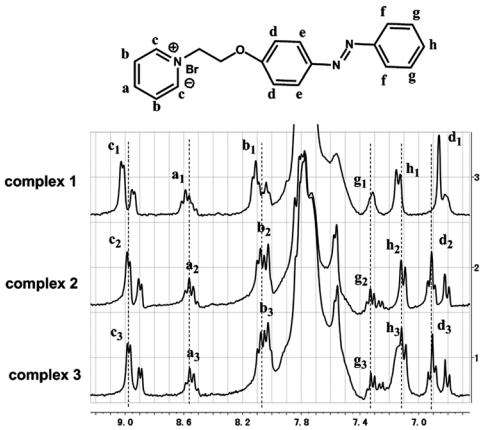

Fig. 3 ^{1}H NMR spectra of (**complex 1**) the proton signals of aromatic rings in the binary system of (AZO + CD-PNIPAM$_{73}$, **complex 2**) proton signals of aromatic rings in the ternary system of (AZO + Te-CD-PNIPAM$_{73}$, **complex 3**) aromatic rings in the ternary system of AZO + Arg-CD-PNIPAM$_{73}$ in D_2O.

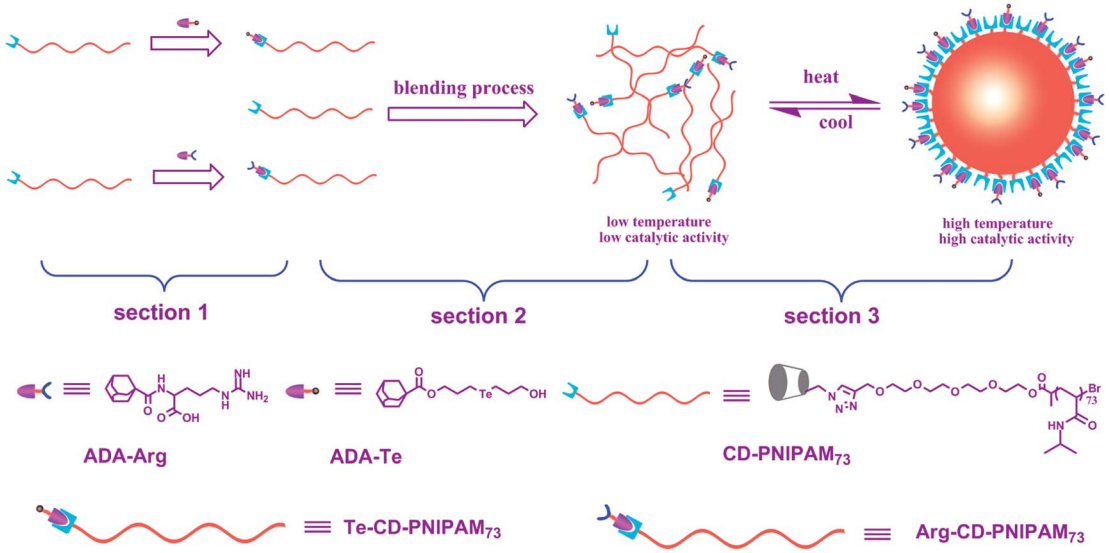

Scheme 1 A graphical representation of SGPx: (section 1) the construction of supramolecular building blocks (Te-CD-PNIPAM$_{73}$, Arg-CD-PNIPAM$_{73}$); (section 2) the construction of SGPx by a blending process; and (section 3) the reversible temperature responsive behavior of SGPx.

the hydrophobic cavity of cyclodextrin and the proton signals were shielded. These results were in line with the previous investigation of the formation mechanism of host–guest complex between **AZO** and functional cyclodextrin.[45,61] Additionally, compared with the proton signals of d_2 and g_2 (or d_3 and g_3) in **complex 2** or **complex 3**, these proton signals in **complex 1** were broad peaks, which also proved that these protons were included in the hydrophobic cavity of cyclodextrin. Similar result was also reported previously.[62] The investigation mentioned above suggested that **AZO** was included in the cavity of cyclodextrin in **complex 1** and was not included in the cavity of cyclodextrin in **complex 2** or **complex 3**. It also proved that the cavity of cyclodextrin in **Te-CD-PNIPAM$_{73}$** or **Arg-CD-PNIPAM$_{73}$** was occupied by adamantane in **ADA-Te** or **ADA-Arg**. Equally, it indirectly confirmed that host–guest complex in **SGPx** was formed.

Moreover, the formation of host–guest complex in **SGPx** was further confirmed by the changes of optical transmittance of various supramolecular building blocks (**CD-PNIPAM$_{73}$**, **Arg-CD-PNIPAM$_{73}$**, **Te-CD-PNIPAM$_{73}$**). As Fig. 4 displayed, the temperature dependence of optical transmittance of various supramolecular building blocks was given. Typically, The LCST of **CD-PNIPAM$_{73}$**, **Arg-CD-PNIPAM$_{73}$**, **Te-CD-PNIPAM$_{73}$** were 34.4 °C, 33.6 °C, 32.8 °C, respectively. Compared with the LCST of **CD-PNIPAM$_{73}$**, the LCST of **Arg-CD-PNIPAM$_{73}$** (34.5 °C) was higher and the LCST of **Te-CD-PNIPAM$_{73}$** (33.4 °C) was lower. It was reported that the LCST of PINPAM could be affected by the anchored functional groups with different hydrophilic–hydrophobic property.[63] Herein, the phenomenon in this work was in good agreement with the previous report. It also proved that host–guest complex in **SGPx** was indeed formed.

Optimizing the structure of smart artificial GPx

It is known that the slight change of the structure will result in dramatic change in catalytic activity for a native enzyme. Herein, both the polymer structure in **SGPx** and the match degree of the catalytic factors in **SGPx** played important roles in influencing the catalytic activity.

In the first place, as the cyclodextrin-containing host polymer (**CD-PNIPAM**) was used as scaffold for artificial **GPx**, it was necessary to reveal the influence of polymer structure on the catalytic activity of artificial **GPx**. Accordingly, three kinds of cyclodextrin-containing host polymers with different molecular weights (**CD-PNIPAM$_{73}$**, **CD-PNIPAM$_{130}$**, **CD-PNIPAM$_{374}$**) were synthesized by ATRP. Combining **CD-PNIPAMs** with **ADA-Te**, three kinds of host–guest artificial **GPxs** (**Te-CD-PNIPAM$_{73}$**, **Te-CD-PNIPAM$_{130}$**, **Te-CD-PNIPAM$_{374}$**) were constructed. Usually, the twine of polymer chain in PNIPAM was more serious when the molecular weight of PNIPAM was larger. Especially, during the temperature responsive process when the temperature was above LCST, the twine of polymer chain in PNIPAM was further enhanced. Therefore, we anticipated that the corresponding catalytic activities of **Te-CD-PNIPAM$_{73}$**, **Te-CD-PNIPAM$_{130}$**, **Te-CD-PNIPAM$_{374}$** could be affected by their different twisting polymer structures related to their different molecular weights.

To confirm this supposition and investigate the catalytic activities of **Te-CD-PNIPAM$_{73}$**, **Te-CD-PNIPAM$_{130}$**, **Te-CD-PNIPAM$_{374}$**, the temperature for the evaluating of catalytic activity was firstly determined by the following way. As Fig. 4a–c shown, the optical transmittance trend to be a fixed value when the temperature was above 36 °C, which proved that the efficient self-assembled aggregation was formed during the temperature responsive process. Considering that self-assembly structure largely affected the catalytic activity of artificial **GPx**,[50] the analysis of the catalytic activities was carried out at 36 °C. For evaluating the catalytic behavior of **Te-CD-PNIPAM$_{73}$**, **Te-CD-PNIPAM$_{130}$**, **Te-CD-PNIPAM$_{374}$**, the catalytic activity for the reduction of cumene hydorperoxide (CUOOH) by 3-carboxyl-4-nitrobenzenethiol (TNB) was evaluated at 36 °C according to the modified method reported by Hilvert *et al.*[12] using TNB as a GSH

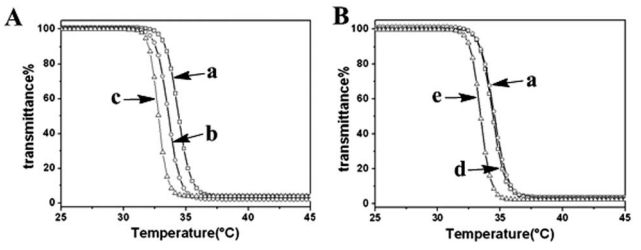

Fig. 4 Temperature dependence of optical transmittance at 600 nm obtained for pH 7.0, 50 mM PBS of (a) CD-PNIPAM$_{73}$, (b) CD-PNIPAM$_{130}$, (c) CD-PNIPAM$_{374}$, (d) Arg-CD-PNIPAM$_{73}$, (e) Te-CD-PNIPAM$_{73}$ at concentration of 1 mg ml^{-1}.

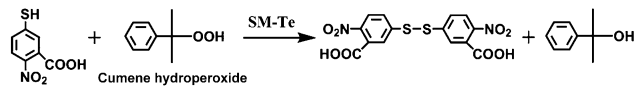

Fig. 5 Determination of GPx activity using 3-carboxyl-4-nitrobenzenethiol (TNB) as a substrate.

Table 2 The initial rates (v_0) and activities for the reduction of hydroperoxides (ROOH) (250 μM) by ArSH in the presence of artificial GPx at pH 7.0 (50 mM PBS) and 36 °C

Catalyst	Temperature (°C)	ArSH	ROOH	v_0[a] (μM min^{-1})
ADA-Arg	36	TNB	CUOOH	0.012
ADA-Te	36	TNB	CUOOH	0.23
CD-PNIPAM$_{73}$	36	TNB	CUOOH	0.046
Arg- CD-PNIPAM$_{73}$	36	TNB	CUOOH	0.018
Te-CD-PNIPAM$_{73}$	36	TNB	CUOOH	2.02
Te-CD-PNIPAM$_{130}$	36	TNB	CUOOH	1.51
Te-CD-PNIPAM$_{374}$	36	TNB	CUOOH	1.41
Arg-Te-CD-PNIPAM$_{73max}$	36	TNB	CUOOH	9.36
CD-Te-CD-PNIPAM$_{73max}$	36	TNB	CUOOH	8.51
SGPx$_{max}$	36	TNB	CUOOH	18.75
SGPx$_{max}$	36	TNB	H_2O_2	4.63
SGPx$_{max}$	36	NBT	CUOOH	8.12
SGPx$_{max}$	36	NBT	H_2O_2	1.26

[a] The concentration of catalyst was 1 μM. And the initial rate of reaction was corrected for the spontaneous oxidation.

alternative (see Fig. 5). The relative activities were summarized in Table 2. From Table 2, we found that the catalytic rates of **Te-CD-PNIPAM$_{73}$**, **Te-CD-PNIPAM$_{130}$**, **Te-CD-PNIPAM$_{374}$** were 2.02 μM min^{-1}, 1.51 μM min^{-1}, 1.41 μM min^{-1}, respectively. The catalytic rates decreased with the increasing molecular weights. This trend might be caused by their different temperature responsive properties related to their different molecular weights. Herein, the investigation of dynamic light scattering (Fig. 6a–c) revealed that the hydrodynamic diameters was larger when the molecular weight was larger. Correspondingly, it meant that the aggregated morphology of **Te-CD-PNIPAM$_{374}$** was larger and the twine structure was much more serious. Under this condition, the catalytic center anchored in **Te-CD-PNIPAM$_{374}$** was easily buried in its twine structure when the temperature was above its LCST. This phenomenon might be responsible for the lower catalytic rate of **Te-CD-PNIPAM$_{374}$** and the higher catalytic rate of **Te-CD-PNIPAM$_{73}$**. Thus, **Te-CD-PNIPAM$_{73}$** was selected as the optimum host building block for the subsequently construction of **SGPx$_{max}$**.

Subsequently, as the match degree of the catalytic factors in **SGPx** might play an important role in influencing the catalytic activity, the construction of optimum supramolecular artificial **GPx** (**SGPx$_{max}$**) was accomplished by a blending process. A graphical representation of the construction of **SGPx$_{max}$** was illustrated in Scheme 1 section 2. Herein, **Te-CD-PNIPAM$_{73}$**, **Arg-CD-PNIPAM$_{73}$**, and **CD-PNIPAM$_{73}$** were functioned as the building blocks for **SGPx$_{max}$**, which endowed **SGPx$_{max}$** with the catalytic center, binding site, and hydrophobic cavity, respectively. Considering that the catalytic activity was crucial important for a successful artificial **GPx**, the data of the catalytic activities were employed as the effective values to reflect the optimization of artificial **GPx** by a blending process. On the one hand, by the blending of building blocks (**Te-CD-PNIPAM$_{73}$** and **Arg-CD-PNIPAM$_{73}$**), **Arg-Te-CD-PNIPAM$_{73}$** modified with catalytic center and binding site was constructed. As shown in Fig. 7A, the component of **Arg-Te-CD-PNIPAM$_{73}$** was optimized by plotting the catalytic rate against the molar ratio of **Arg-CD-PNIPAM$_{73}$** to **Te-CD-PNIPAM$_{73}$**. It was noticeable that the catalytic rate of **Arg-CD-PNIPAM$_{73}$** increased to some extent with the molar ratio going up. And it reached the highest value (see Table 2, **Arg-CD-PNIPAM$_{73max}$** = 9.36 μM min^{-1}) when the molar ratio was 6 : 1. However, the catalytic rate decreased when the molar ratio increased further. For **Arg-CD-PNIPAM$_{73}$**, the better match between catalytic center and binding site would result in the stronger substrate binding ability and higher catalytic activity. Thus, the highest catalytic activity was obtained when the best match was achieved with the molar ratio was 6 : 1. However, the enhanced binding ability could bind much more substrates in a distribution away from the catalytic center and made the completion of catalytic cycle in an inefficient way. Therefore, the decreased catalytic rate was observed when the molar ratio was increased further. Similar results were also reported in our previous work.[50] On the other hand, using the same protocol as mentioned above, the component of **CD-Te-CD-PNIPAM$_{73}$** was optimized by plotting the catalytic rate against the molar ratio of **CD-PNIPAM$_{73}$** to **Te-CD-PNIPAM$_{73}$** (see Fig. 7B). And the highest catalytic rate (see Table 2, **CD-Te-CD-PNIPAM$_{73max}$** = 8.51 μM min^{-1}) was achieved when the molar ratio of **CD-PNIPAM$_{73}$** to **Te-CD-PNIPAM$_{73}$** was 5 : 1.

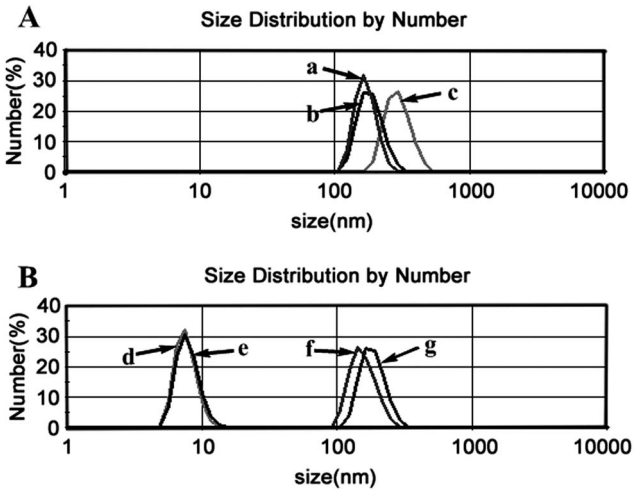

Fig. 6 (A) Hydrodynamic diameters of CD-PNIPAM$_{73}$ (a), CD-PNIPAM$_{130}$ (b), and CD-PNIPAM$_{374}$ (c) at 36 °C determined using a Malvern ZETAS12-ERNANOSERIES instrument; (B) hydrodynamic diameters of SGPx$_{max}$ at varying temperature (25 °C (d); 32 °C (e); 36 °C (f); 40 °C (g)).

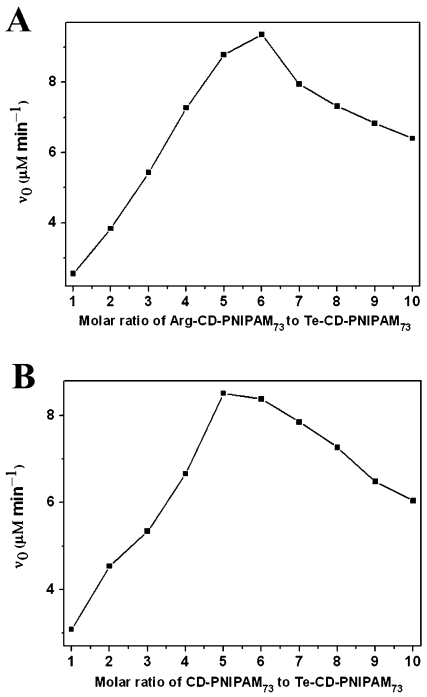

Fig. 7 Plots of catalytic rates v_0 against molar ratio of functional copolymer: (A), Arg-CD-PNIPAM$_{73}$ to Te-CD-PNIPAM$_{73}$ (The concentration of Te-CD-PNIPAM$_{73}$ was 1 μM. The concentrations of Arg-CD-PNIPAM$_{73}$ were 1, 2, 3, 4, 5, 6, 7, 8, 9, and 10 μM, respectively); (B) CD-PNIPAM$_{73}$ to Te-CD-PNIPAM$_{73}$. (The concentration of Te-CD-PNIPAM$_{73}$ was 1 μM. The concentrations of CD-PNIPAM$_{73}$ were 1, 2, 3, 4, 5, 6, 7, 8, 9, and 10 μM, respectively).

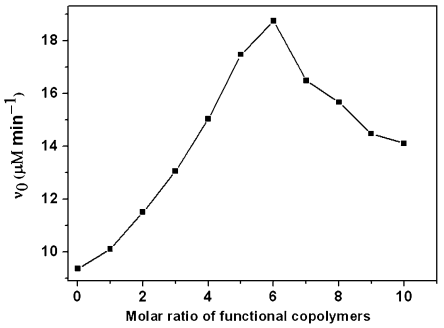

Fig. 8 Plots of catalytic rates v_0 against molar ratio of functional copolymer: (a) **CD-PNIPAM$_{73}$** to **Te-CD-PNIPAM$_{73}$** (the ratio of **Arg-CD-PNIPAM$_{73}$** to **Te-CD-PNIPAM$_{73}$** was fixed to 6 : 1). (The concentration of **Te-CD-PNIPAM$_{73}$** was 1 μM. The concentrations of **Arg-CD-PNIPAM$_{73}$** was 6 μM. The concentrations of **CD-PNIPAM$_{73}$** were 0, 1, 2, 3, 4, 5, 6, 7, 8, 9, and 10 μM, respectively).

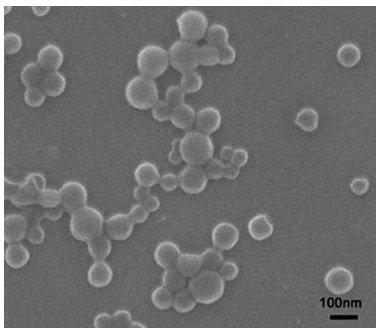

Fig. 9 SEM image for **SGPx$_{max}$**.

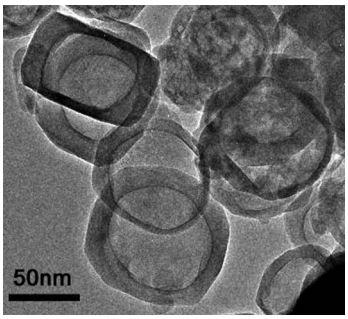

Fig. 10 TEM image for **SGPx$_{max}$**.

Finally, the optimum **SGPx** was achieved using a blending process based on **Te-CD-PNIPAM$_{73}$**, **Arg-CD-PNIPAM$_{73}$**, and **CD-PNIPAM$_{73}$**. As displayed in Fig. 8, the molar ratio of **Arg-CD-PNIPAM$_{73}$** to **Te-CD-PNIPAM$_{73}$** was fixed to 6 : 1 and the molar ratio of **CD-PNIPAM$_{73}$** to **Te-CD-PNIPAM$_{73}$** was altered. Ultimately, the best match of catalytic factors was achieved by altering the molar ratio of three functional supramolecular polymers. The optimum **SGPx** (see Table 2, **SGPx$_{max}$** = 18.75 μM min^{-1}) with the highest catalytic rate was successfully constructed when the molar ratio was 6 : 6 : 1. Now, we can draw a conclusion that the construction of **SGPx$_{max}$** was achievable through altering the molar ratio of three functional supramolecular polymers by a blending process.

Considering that detailed information of aggregated behavior of **SGPx$_{max}$** was important to reveal its catalytic mechanism, its detailed aggregated behavior was investigated based on dynamic light scattering, SEM, TEM and the temperature dependence of optical transmittance. As shown in Fig. 6B, the hydrodynamic diameters of **SGPx$_{max}$** in aqueous solutions were typically 7 nm when the temperature was lower than the LCST of **SGPx$_{max}$** (curve d, curve e). Nevertheless, the corresponding hydrodynamic diameters shifted to larger than 100 nm when the temperature was higher than the LCST of **SGPx$_{max}$** (curve f, curve g). Considering that the hydrophilic PNIPAM block was changed to hydrophobic in different degree at corresponding temperature, the changes of the diameters of **SGPx$_{max}$** might be derived from the different assembled structures that were formed at corresponding temperatures. Similar phenomenon was also reported in our previous reports.[16,50] Furthermore, the actual morphology of **SGPx$_{max}$** at 36 °C was observed by SEM in Fig. 9. We could clearly see that the presence of spherical nanoparticles of 80–100 nm in diameters. As SEM shown, the dimensions of these nanoparticles in the dry state were reasonably smaller than those detected by a Zetasizer Nano instrument at the same temperature, since the Zetasizer Nano instrument provided the average hydrophobic diameter of nanoparticles in solution which contained the contribution from the swollen corona. Moreover, from the TEM image in Fig. 10, we found that the nanoparticles were hollow vesicle-like nanoparticles with a thinner region surrounded by a thicker region and clearly confirmed the boundary between the thinner and the thicker ones. Similar behavior has been reported by Chen and coworkers.[64] Additionally, as Fig. 11 shown, the temperature dependence of optical transmittance of **SGPx$_{max}$** was given. Its LCST was 34.4 °C.

Catalytic behavior of SGPx$_{max}$

The catalytic activity of **SGPx$_{max}$** was investigated using TNB as a GSH alternative. Normally, the reaction between CUOOH and TNB was very slow under the spontaneous oxidation condition. To evaluate the effluence of the catalytic activity by supramolecular scaffold, the control experiments were carried out. Typically, the catalytic activity of **ADA-Arg**, **ADA-Te**,

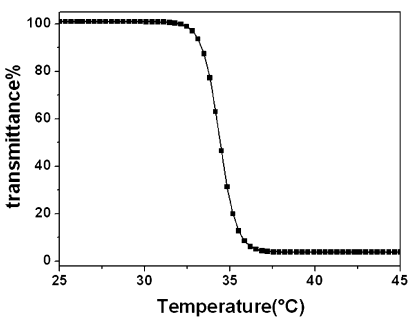

Fig. 11 Temperature dependence of optical transmittance at 600 nm obtained for pH 7.0, 50 mM PBS of **SGPx$_{max}$** at concentration of 1 mg ml^{-1}.

CD-PNIPAM$_{73}$ and **Arg-CD-PNIPAM$_{73}$** were determined using the similar assay method of other artificial enzyme (see Table 2). From Table 2, it was concluded that the reaction between CUOOH and TNB under the catalytic oxidation condition were relative lower. However, a remarkable rate enhancement (**SGPx$_{max}$** = 18.75 μM min^{-1}) was observed under the identical condition when **SGPx$_{max}$** was added. This observation not only proved that the catalytic activities derived from the supramolecular scaffold were slight but also suggested that the remarkable catalytic activity can be obtained by assembly and blend of various catalytic element (catalytic center and binding site). Additionally, seen from Fig. 12, the saturation kinetic of **SGPx$_{max}$** for the peroxidase reaction was studied at the individual concentrations of CUOOH, which indicated that **SGPx$_{max}$** exhibited typical saturation kinetics and acted as a real catalyst for peroxidase reaction. In the TNB assay system, the apparent kinetic parameters were obtained: V_{max} = 85.62 μM min^{-1}, k_{cat}^{app} = 85.62 min^{-1}, K_{mCUOOH} = 907.53 μM, k_{cat}^{app}/K_{mCUOOH} = 9.43 × 10^4 M^{-1} min^{-1}, and the turnover number per catalytic center tellurium was calculated to be 86 min^{-1}.

For an efficient artificial enzyme, the strong substrates binding ability was one of the most important characteristics. For native **GPx**, the binding site (formed between two arginines and carboxylic group of GSH) and the hydrophobic cavity (composed of some hydrophobic amino residues) played important roles in binding substrates and maintaining the efficient catalytic activity. For **SGPx$_{max}$** constructed in this work, similar binding site and hydrophobic cavity were also incorporated. Herein, the binding site was derived from the arginine residue in **ADA-Arg**. And the cavity of cyclodextrin in **CD-PNIPAM$_{73}$** could effectively recognize aromatic thiol substrates being similar to the hydrophobic cavity in native **GPx**. Consequently, the best match degree of catalytic factors (catalytic center, binding site, and hydrophobic cavity) might endow **SGPx$_{max}$** with strong and special substrates binding ability. Equally, it would also play an important role in maintaining the efficient catalytic activity.

To confirm the interaction between the substrate TNB and **SGPx$_{max}$**, UV spectrum were employed to check the substrate binding ability. It was known that the maximum absorbance wavelength of TNB was 410 nm in aqueous solution (pH = 7.0), and it would appear as a red shift when it was in a hydrophobic microenvironment. Fig. 13 illustrated the UV spectra of the assayed mixtures with various amounts of **SGPx$_{max}$**. As expected, a red shift of maximum absorbance wavelength was observed, which indicated that a strong hydrophobic interaction existed between the aryl moiety of TNB and the binding sites of **SGPx$_{max}$**. In other words, **SGPx$_{max}$** could exhibit the strong substrates binding ability during the **GPx** catalytic process. To further confirm the substrate binding ability of **SGPx$_{max}$**, the catalytic rates were measured in different assay systems (shown in Fig. 14): CUOOH, TNB assay system (Fig. 14A), v_0 = 18.75 μM min^{-1}; CUOOH, NBT assay system (Fig. 14B), v_0 = 8.12 μM min^{-1}; H_2O_2, TNB assay system (Fig. 14C), v_0 = 4.63 μM min^{-1}; H_2O_2, NBT assay system (Fig. 14D), v_0 = 1.26 μM min^{-1}. It was found that much lower catalytic rate was observed when NBT was used as substrate (B < A or D < C). The difference between NBT and TNB was that NBT was a smaller molecule in size than TNB owing to the lack of a carboxyl function group in NBT. Considering that the similar assay condition (only substrates TNB and NBT were different) was used in two assay systems, the dramatic change in the catalytic activities should be mainly derived from the electrostatic interaction that was formed between the carboxyl in TNB and arginine in **SGPx$_{max}$**. Furthermore, the catalytic rates were measured under same condition except the different ROOHs (CUOOH and H_2O_2) were used. The difference between CUOOH and H_2O_2 was that CUOOH was a more hydrophobic substrate than H_2O_2 owing to the presence of the hydrophobic cumenyl

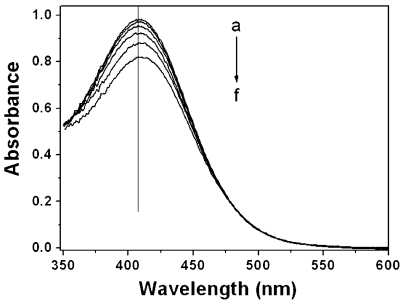

Fig. 13 UV spectra with varying concentration of SGPx$_{max}$ in water; the concentration of TNB was 68 μM, and from a to f the concentrations of SGPx$_{max}$ were 0, 0.2, 0.4,1, 1.5, and 4 mM, respectively.

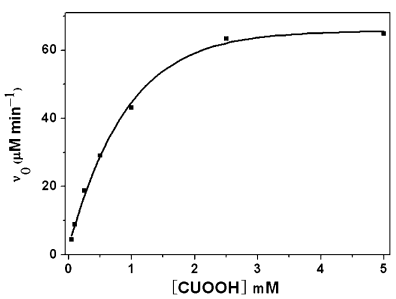

Fig. 12 Plots of initial rates at different concentrations of CUOOH in the presence of SGPx$_{max}$. The initial concentration of TNB was fixed to 0.15 mM, The concentrations of CUOOH were 0.05, 0.10, 0.25, 0.5, 1, 2.5 and 5 mM, respectively.

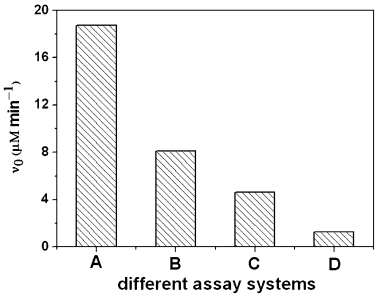

Fig. 14 The catalytic rates (v_0) for the reduction of hydroperoxides (250 μM) by TNB and NBT (150 μM) in the presence of SGPx$_{max}$ at pH 7.0 (50 mM PBS) and 36 °C. (A) CUOOH, TNB; (B) CUOOH, NBT; (C) H_2O_2, TNB; (D) H_2O_2, NBT.

group in CUOOH. Usually, the rate constants of the spontaneous reaction between hydroperoxide and thiol vary in magnitude in the order $k(H_2O_2) > k(CUOOH)$.[7] However, by comparing the assay system A and C (or B and D), it was noticeable that the catalytic activity of **SGPx$_{max}$** exhibited a significant enhancement when CUOOH as a substrate instead of H_2O_2. This difference in catalytic activities was mainly because that the hydrophobic microenvironment in **SGPx$_{max}$** enabled the hydrophobic substrate CUOOH to approach **SGPx$_{max}$** easier and complete the catalytic cycle more preferentially.

Consequently, based the above experiments, we could conclude that **SGPx$_{max}$** was endowed with strong substrate binding ability through both electrostatic interaction and hydrophobic interaction, which was derived from **Arg-CD-PNIPAM$_{73}$** and **CD-PNIPAM$_{73}$** respectively. And the stronger substrate binding ability further resulted in higher catalytic rates.

Temperature responsive catalytic behavior of SGPx$_{max}$

The temperature responsive property of **SGPx$_{max}$** was investigated by assaying the catalytic activities in TNB assay system using CUOOH as a substrate at various temperatures from 25 °C to 45 °C. To our knowledge, for the majority of temperature-activated reactions, the reaction rates would be enhanced with rising temperature according to Arrhenius equation. However, it was different for **SGPx$_{max}$**. Herein, a thermal-responsible catalytic activity curve was obtained by plotting the catalytic rate against temperature (Fig. 15).

It was observed that the catalytic activity increased slowly with the increasing temperature when the temperature was lower than 33 °C, and it increased remarkably with the temperature increasing from 33 °C to 36 °C. Furthermore, when the temperature increased higher above 36 °C, the catalytic activity increased slowly again. Benefited from the presence of PNIPAM scaffold, **SGPx$_{max}$** exhibited the typical temperature responsive behavior. In the section *optimizing the structure of smart artificial* **GPx** mentioned above, the detailed information of aggregated behavior of **SGPx$_{max}$** during the temperature responsive process was investigated. We speculated that the temperature responsive catalytic activity of **SGPx$_{max}$** was endowed by the change of the self-assembled structure of **SGPx$_{max}$** during the temperature responsive process. To explicate the temperature responsive catalytic mechanism, the hydrodynamic diameters of the self-assembled structures of **SGPx$_{max}$** were assayed at various temperatures and the temperature dependence of optical transmittance of **SGPx$_{max}$** was measured with the increasing temperature. A graphical representation of the temperature responsive catalytic mechanism was illustrated in Scheme 1 section 3.

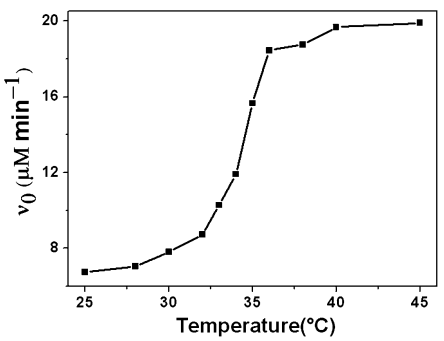

Fig. 15 Plots of the catalytic rate of SGPx$_{max}$ (1.00 μM) *versus* temperature during the catalytic reduction of CUOOH (0.25 mM) by TNB (0.15 mM).

Typically, PNIAPM exhibited the lower critical solution temperature (LCST) of about 32 °C. A great deal of hydrogen bonds between amide group and surrounding water molecules were formed when the temperature was lower than its LCST, which enabled the PNIPAM block totally dissolve in water. However, the hydrophilic PNIAM block changed to hydrophobic block to different degree when different amounts of hydrogen bonds were cleaved during the temperature responsive process. Usually, accompanied with break of hydrogen bonds, the self-assembled structures were formed as the hydrophobic PNIAM block aggregating together in water. And such phenomenon was also observed in the temperature responsive process of **SGPx$_{max}$** (its LCST was 34.4 °C). As displayed in Fig. 11, the temperature dependence of optical transmittance of **SGPx$_{max}$** was measured at various temperatures from 25 °C to 45 °C. It was noticeable that the optical transmittance of **SGPx$_{max}$** was nearly 100% below 33 °C, which indicated that **SGPx$_{max}$** was dissolved in water and the PNIAPM block was hydrophilic. Moreover, as shown in Fig. 6B(d) and (e), the hydrodynamic diameters of **SGPx$_{max}$** were smaller than 10 nm when the temperature was lower than its LCST, which also indicated that **SGPx$_{max}$** was hydrophilic and was dissolved in water. This observation was in close agreement with the analysis of the temperature dependences of optical transmittance of **SGPx$_{max}$**. Herein, for **SGPx$_{max}$**, the catalytic factors were incorporated into the supramolecular blocks. Therefore, the supramolecular blocks accompanied with catalytic factors were distributed in a randomly manner in water when the temperature was lower than its LCST. And the good match of the catalytic factors could not be easily achieved, which further resulted in a lower catalytic activity.

Subsequently, the sharp decrease in optical transmittance was observed in Fig. 11 when the temperature was higher than 33 °C. The optical transmittance of **SGPx$_{max}$** became much lower with the increasing temperature, which indicated that the PNIPAM block of **SGPx$_{max}$** became hydrophobic due to the cleavage of hydrogen bonds. Meanwhile, the self-assembled structures were formed as the shift of PNIPAM in **SGPx$_{max}$** form hydrophilic to hydrophobic. From Fig. 6B(f) and (g), the increased hydrodynamic diameters of **SGPx$_{max}$** (larger than 100 nm) were observed when the temperature was higher than its LCST, which was in agreement with the conclusion from the changes of optical transmittance. Combing the detailed information of aggregated behavior from Fig. 9 and 10, it was concluded that self-assembled vesicles were formed when the PNIPAM block of **SGPx$_{max}$** changed from hydrophilic to hydrophobic. It is well known that a minor change of the structure of

the enzyme will result in a dramatic change in activity for naturally occurring enzymes. Herein, the remarkable changes of aggregated behavior of **SGPx$_{max}$** also resulted in a dramatic change in catalytic activity. As shown in Fig. 15, the curve of thermal-responsible catalytic activity was obtained by plotting the catalytic rate against temperature. The catalytic rate increased remarkably with the temperature increasing from 33 °C to 36 °C. Under these conditions, the PNIPAM block of **SGPx$_{max}$** was hydrophobic and the self-assembled vesicles were formed. Consequently, the catalytic factors in **SGPx$_{max}$** were concentrated in the vesicle, which resulted in the distance among the catalytic factors in vesicle was much closer. Accordingly, the better match of the catalytic factors could be easily achieved. Then, it enabled the catalytic cycle completed in an efficient way. Thus, as the better match of the catalytic factors were achieved with the temperature increasing from 33 °C to 36 °C, the largely enhancement of the catalytic activity was observed.

However, the catalytic activities increased slowly again when the temperature increased higher above 36 °C. It was apparent that the optical transmittance of **SGPx$_{max}$** was stable when the temperature was above 36 °C (see Fig. 11), which meant the stable vesicles have aggregated under these conditions. As the cyclodextrin was anchored into **CD-PNIPAMs** as the end group, the catalytic factors were presented as the hydrophilic block at the end of functional building blocks (**CD-PNIPAM$_{73}$**, **Te-CD-PNIPAM$_{73}$**, **Arg-CD-PNIPAM$_{73}$**). Therefore, as illustrated in Scheme 1 section 3, these catalytic factors might be assembled on the surface of the aggregated vesicles as their hydrophilicity. Once the vesicle was formed, the distance of the catalytic factors would be slightly changed and the match degree of the catalytic factor changed to the steady state even if the temperature was further increased. Therefore, the substrates binding ability was also slightly changed and the catalytic activity was increased more slowly. Additionally, as shown in Fig. 6B, the hydrodynamic diameter of **SGPx$_{max}$** was further increased at the higher temperature (g > f). It might be caused by the reason that the larger aggregated structure could be assembled by universal vesicles at higher temperature as the hydrophobicity of the PNIPAM became stronger, which was also reported in previous reported.[14] Under this condition, some catalytic factors might be buried in the scaffold of the larger aggregated structure, which would play a role in the slowly increasing of catalytic activity to some extent.

Now we can draw a conclusion that the change of the self-assembled structure of **SGPx$_{max}$** during the temperature responsive process plays a significant role in the altering of the temperature responsive catalytic activity.

Conclusions

In this work, a novel smart artificial **GPx** (**SGPx**) was prepared *via* host–guest interaction and a blending process for the first time. Herein, the functional guest molecules (**ADA-Te** and **ADA-Arg**) and the cyclodextrin-containing host polymers (**CD-PNIPAMs**) were synthesized. And the optimum host building block (**CD-PNIPAM$_{73}$**) was selected. Significantly, the optimum supramolecular artificial **GPx** (**SGPx$_{max}$**) with vesicles structure was achieved through altering the molar ratio of building blocks (**CD-PNIPAM$_{73}$**, **ADA-Te**, **ADA-Arg**). The catalytic rates of **SGPx$_{max}$** displayed a noticeable temperature responsive characteristic and **SGPx$_{max}$** exhibited the typical saturation kinetics behavior as a real enzyme catalyst. It was proved that the change of the self-assembled structure of **SGPx$_{max}$** during the temperature responsive process played a significant role in altering the temperature responsive catalytic behavior. We anticipate that this study would not only overcome the insurmountable disadvantages existed in traditional supramolecular artificial **GPx** but also open up a new field in designing other smart antioxidative artificial enzyme. And we also hope this prepared process could highlight the preparation of other biologically related functional supramolecular materials.

Acknowledgements

This research was supported by financial support from the Natural Science Foundation of China (no: 51303088, 51203082, 21234004), the Natural Science Foundation of Guangxi Province (no. 2013GXNSFBA019043), the Natural Science Foundation of Education Bureau of Guangxi Province (no. 2013YB254).

Notes and references

1 H. Sies, Oxidative Stress: Introductory Remarks, in *Oxidative Stress*, ed. H. Sies, Academic Press, London, 1985, p. 1.
2 H. Sies, *Angew. Chem., Int. Ed.*, 1986, **25**, 1058–1071.
3 H. Sies, *Exp. Physiol.*, 1997, **82**, 291–295.
4 O. Epp, R. Ladenstein and A. Wendel, *Eur. J. Biochem.*, 1983, **133**, 51–69.
5 L. Flohé, G. Loschen, W. A. Günzler and E. Eichele, *Hoppe-Seyler's Z. Physiol. Chem.*, 1972, **353**, 987–999.
6 T. G. Back and Z. Moussa, *J. Am. Chem. Soc.*, 2003, **125**, 13455–13460.
7 Z. Y. Dong, J. Q. Liu, S. Z. Mao, X. Huang, B. Yang, X. J. Ren, G. M. Luo and J. C. Shen, *J. Am. Chem. Soc.*, 2004, **126**, 16395–16404.
8 L. Engman, D. Stern, I. A. Cotgreave and C. M. Andersson, *J. Am. Chem. Soc.*, 1992, **114**, 9737–9743.
9 C. X. Hou, J. X. Li, L. L. Zhao, W. Zhang, Q. Luo, Z. Y. Dong, J. Y. Xu and J. Q. Liu, *Angew. Chem., Int. Ed.*, 2013, **52**, 5590–5593.
10 C. X. Hou, Q. Luo, J. Q. Liu, L. Miao, C. Q. Zhang, Y. Z. Gao, X. Y. Zhang, J. Y. Xu, Z. Y. Dong and J. Q. Liu, *ACS Nano*, 2012, **6**, 8692–8701.
11 G. Mugesh and H. B. Singh, *Chem. Soc. Rev.*, 2000, **29**, 347–357.
12 Z. P. Wu and D. Hilvert, *J. Am. Chem. Soc.*, 1990, **112**, 5647–5648.
13 Z. Y. Dong, Y. G. Wang, Y. Z. Yin and J. Q. Liu, *Curr. Opin. Colloid Interface Sci.*, 2011, **16**, 451–458.
14 X. Huang, Y. Z. Yin, X. Jiang, Y. Tang, J. Y. Xu, J. Q. Liu and J. C. Shen, *Macromol. Biosci.*, 2009, **9**, 1202–1210.
15 X. Huang, Y. Z. Yin, Y. Liu, X. L. Bai, Z. M. Zhang, J. Y. Xu, J. C. Shen and J. Q. Liu, *Biosens. Bioelectron.*, 2009, **25**, 657–660.

16 X. Huang, Y. Z. Yin, Y. Tang, X. L. Bai, Z. M. Zhang, J. Y. Xu, J. Q. Liu and J. C. Shen, *Soft Matter*, 2009, **5**, 1905–1911.
17 S. J. Yu, X. Huang, L. Miao, J. Y. Zhu, Y. Z. Yin, Q. Luo, J. Y. Xu, J. C. Shen and J. Q. Liu, *Bioorg. Chem.*, 2010, **38**, 159–164.
18 S. J. Yu, W. Zhang, J. Y. Zhu, Y. Z. Yin, H. Y. Jin, L. P. Zhou, Q. Luo, J. Y. Xu and J. Q. Liu, *Macromol. Biosci.*, 2011, **11**, 821–827.
19 S. J. Yu, Y. Z. Yin, J. Y. Zhu, X. Huang, Q. Luo, J. Y. Xu, J. C. Shen and J. Q. Liu, *Soft Matter*, 2010, **6**, 5342–5350.
20 Y. Z. Yin, X. Huang, C. Y. Lv, L. Wang, S. J. Yu, Q. Luo, J. Y. Xu and J. Q. Liu, *Macromol. Biosci.*, 2010, **10**, 1505–1516.
21 Y. Tang, L. P. Zhou, J. X. Li, Q. Luo, X. Huang, P. Wu, Y. G. Wang, J. Y. Xu, J. C. Shen and J. Q. Liu, *Angew. Chem., Int. Ed.*, 2010, **49**, 3920–3924.
22 H. Y. Wang, L. Wang, X. G. Wang, J. Y. Xu, Q. Luo and J. Q. Liu, *New J. Chem.*, 2011, **35**, 2632–2638.
23 A. Klug, *Angew. Chem., Int. Ed.*, 1983, **22**, 565–582.
24 J. M. Lehn, *Science*, 2002, **295**, 2400–2403.
25 C. Casati, P. Franchi, R. Pievo, E. Mezzina and M. Lucarini, *J. Am. Chem. Soc.*, 2012, **134**, 19108–19117.
26 J. M. Lehn, *Chem. Soc. Rev.*, 2007, **36**, 151–160.
27 J. M. Lehn, *Chem.–Eur. J.*, 1999, **5**, 2455–2463.
28 T. Ogoshi, Y. Takashima, H. Yamaguchi and A. Harada, *J. Am. Chem. Soc.*, 2007, **129**, 4878–4879.
29 H. Yang, H. Chen and Y. B. Tan, *RSC. Adv.*, 2013, **3**, 3031–3037.
30 R. Bappaditya, B. Partha and K. N. Arun, *RSC. Adv.*, 2014, **4**, 1708–1734.
31 D. L. Wang, X. Y. Huan, L. J. Zhu, J. Y. Liu, F. Qiu, D. Y. Yan and X. Y. Zhu, *RSC. Adv.*, 2012, **2**, 11953–11962.
32 C. C. Neikirk, J. W. Chung and R. D. Priestley, *RSC. Adv.*, 2013, **3**, 16686–16696.
33 Y. Bai, Q. Luo, W. Zhang, L. Miao, J. Xu, H. Li and J. Liu, *J. Am. Chem. Soc.*, 2013, **135**, 10966–10969.
34 T. Kubori, Y. Matsushima, D. Nakamura, J. Uralil, M. Lara-Tejero, A. Sukhan, J. E. Galán and S. I. Aizawa, *Science*, 1998, **280**, 602–605.
35 P. Díez, R. Villalonga, M. L. Villalonga and J. M. Pingarrón, *J. Colloid Interface Sci.*, 2012, **386**, 181–188.
36 S. M. Reddy, Q. T. Phan, H. E. Sharif, L. Govada, D. Stevenson and N. E. Chayen, *Biomacromolecules*, 2012, **13**, 3959–3965.
37 L. Tan, Y. Liu, W. Ha, L. S. Ding, S. L. Peng, S. Zhang and B. J. Li, *Soft Matter*, 2012, **8**, 4746–4749.
38 J. Li, X. Li, X. Ni, X. Wang, H. Li and K. W. Leong, *Biomaterials*, 2006, **27**, 4132–4140.
39 J. Yu, H. Fan, J. Huang and J. Chen, *Soft Matter*, 2011, **7**, 7386.
40 M. J. Robb, L. A. Connal, B. F. Lee, N. A. Lynd and C. J. Hawker, *Polym. Chem.*, 2012, **3**, 1618–1628.
41 B. Karagoz, L. Esser, H. T. Duong, J. S. Basuki, C. Boyer and T. P. Davis, *Polym. Chem.*, 2014, **5**, 350–355.
42 A. Harada, R. Kobayashi, Y. Takashima, A. Hashidzume and H. Yamaguchi, *Nat. Chem.*, 2010, **3**, 34–37.
43 M. Nakahata, Y. Takashima, H. Yamaguchi and A. Harada, *Nat. Commun.*, 2011, **2**, 511.
44 J. Q. Liu, G. M. Luo, S. J. Gao, K. Zhang, X. F. Chen and J. C. Shen, *Chem. Commun.*, 1999, 199–200.
45 Y. Z. Yin, S. F. Jiao, C. Lang and J. Q. Liu, *Soft Matter*, 2014, **10**, 3374–3385.
46 Z. Y. Dong, Q. Luo and J. Q. Liu, *Chem. Soc. Rev.*, 2012, **41**, 7890–7908.
47 Y. Z. Yin, Z. Y. Dong, Q. Luo and J. Q. Liu, *Prog. Polym. Sci.*, 2012, **37**, 1476–1509.
48 L. Yu, K. Dean and L. Li, *Prog. Polym. Sci.*, 2006, **31**, 576–602.
49 E. S. Gil, D. J. Frankowski, M. K. Bowman, A. O. Gozen, S. M. Hudson and R. J. Spontak, *Biomacromolecules*, 2006, **7**, 728–735.
50 Y. Z. Yin, L. Wang, H. Y. Jin, C. Y. Lv, S. J. Yu, X. Huang, Q. Luo, J. Y. Xu and J. Q. Liu, *Soft Matter*, 2011, **7**, 2521–2529.
51 C. Koopmans and H. Ritter, *Macromolecules*, 2008, **41**, 7418–7422.
52 M. Ciampolini and N. Nardi, *Inorg. Chem.*, 1966, **5**, 41–44.
53 G. Masci, L. Giacomelli and V. Crescenzi, *Macromol. Rapid Commun.*, 2004, **25**, 559–564.
54 T. M. Eggenhuisen, C. R. Becer, M. W. Fijten, R. Eckardt, R. Hoogenboom and U. S. Schubert, *Macromolecules*, 2008, **41**, 5132–5140.
55 J. Wang and K. Matyjaszewski, *J. Am. Chem. Soc.*, 1995, **117**, 5614–5615.
56 K. Matyjaszewski and J. Xia, *Chem. Rev.*, 2001, **101**, 2921–2990.
57 D. G. Lessard, M. Ousalem and X. X. Zhu, *Can. J. Chem.*, 2001, **79**, 1870–1874.
58 Y. Xia, X. Yin, N. A. D. Burke and H. D. H. Stöver, *Macromolecules*, 2005, **38**, 5937–5943.
59 C. Alexander and K. M. Shakesheff, *Adv. Mater.*, 2006, **18**, 3321–3328.
60 T. Rossow, S. Bayer, R. Albrecht, C. C. Tzschucke and S. Seiffert, *Macromol. Rapid Commun.*, 2013, **34**, 1401–1407.
61 P. Wu, R. Xiao, C. Zhang, L. Zhou, Q. Luo, J. Xu and J. Liu, *Catal. Lett.*, 2010, **138**, 62–67.
62 X. Liao, G. Chen, X. Liu, W. Chen, F. Chen and M. Jiang, *Angew. Chem.*, 2010, **122**, 4511–4515.
63 H. Ringsdorf, J. Venzmer and F. Winnik, *Macromolecules*, 1991, **24**, 1678–1686.
64 M. Hua, T. Kaneko, X. Liu, M. Q. Chen and M. Akashi, *Polym. J.*, 2005, **37**, 59–64.

